Developmental stage-dependent transcriptional regulatory pathways control neuroblast lineage progression

Guoxin Feng*, Peishan Yi*, Yihong Yang*, Yongping Chai*, Dong Tian*, Zhiwen Zhu, Jianhong Liu, Fanli Zhou, Ze Cheng, Xiangming Wang, Wei Li and Guangshuo Ou‡

SUMMARY

Neuroblasts generate neurons with different functions by asymmetric cell division, cell cycle exit and differentiation. The underlying transcriptional regulatory pathways remain elusive. Here, we performed genetic screens in *C. elegans* and identified three evolutionarily conserved transcription factors (TFs) essential for Q neuroblast lineage progression. Through live cell imaging and genetic analysis, we showed that the storkhead TF HAM-1 regulates spindle positioning and myosin polarization during asymmetric cell division and that the PAR-1-like kinase PIG-1 is a transcriptional regulatory target of HAM-1. The TEAD TF EGL-44, in a physical association with the zinc-finger TF EGL-46, instructs cell cycle exit after the terminal division. Finally, the Sox domain TF EGL-13 is necessary and sufficient to establish the correct neuronal fate. Genetic analysis further demonstrated that HAM-1, EGL-44/EGL-46 and EGL-13 form three transcriptional regulatory pathways. We have thus identified TFs that function at distinct developmental stages to ensure appropriate neuroblast lineage progression and suggest that their vertebrate homologs might similarly regulate neural development.

KEY WORDS: *C. elegans*, Asymmetric cell division, Neuroblast development

INTRODUCTION

Neuroblast lineage progression is a fundamental biological process in which neural stem cells asymmetrically divide, exit the cell cycle and differentiate into distinct neurons. Defects in neuroblast lineage progression cause abnormal neural circuits and neurological disorders (Ming and Song, 2011; Zhao et al., 2008). Despite recent progress in understanding the transcriptional control of neurogenesis (Hsieh, 2012), the full inventory of transcription factors (TFs) and regulatory networks underlying neuroblast development remains largely unknown.

The *C. elegans* Q neuroblasts divide three times to generate three distinct neurons (oxygen sensory, mechanosensory and interneuron) and two apoptotic cells in L1 larvae (Fig. 1A) (Sulston and Horvitz, 1977). The anterior and posterior daughters of Q neuroblasts, Q.a and Q.p, employ distinct cellular mechanisms in their asymmetric divisions (Ou et al., 2010). A polarization of myosin-based contractility is the primary driver for the production of two distinct daughter cells in Q.a division (Ou et al., 2010), and the myosin polarization also occurs in *Drosophila* neuroblast asymmetric division (Cabernard et al., 2010). In Q.p division, asymmetric daughter cell sizes and fates arise from the initial displacement of the mitotic spindle towards one side of the cell, which is similar to what occurs in the first division of the *C. elegans* embryo (Gönczy, 2008; Ou et al., 2010). Pioneering *C. elegans* genetics uncovered that a POU domain TF, UNC-86, acts to modify latent reiterative cell lineages of the Q neuroblast; Q.a divides normally but Q.p repeats the division pattern of the mother neuroblast in *unc-86* mutants (Chalfie et al., 1981). Additional transcriptional regulatory

pathways that determine the distinct Q cell division patterns (e.g. Q.a division) have yet to be identified.

Neuroblast division needs to be precisely regulated. In Q neuroblasts, Q.a only divides once whereas Q.p divides twice (Sulston and Horvitz, 1977). The Hippo signaling pathway consists of a core kinase cascade that controls organ size and the development of human cancers. Upon activation in *Drosophila*, Hippo kinase phosphorylates and activates Warts kinase, which inactivates Yorkie by phosphorylation; Yorkie is a transcriptional coactivator of a TEA domain (TEAD) family TF, Scalloped, which induces gene transcription to promote cell proliferation and inhibit apoptosis (Pan, 2010; Zhao et al., 2011). In *C. elegans*, CST-1/2, WTS-1, YAP-1 and EGL-44 are homologs to Hippo, Warts, Yorkie and Scalloped, respectively, and they play diverse roles in life span, development and neuronal fate determination (Cai et al., 2009; Iwasa et al., 2013; Kang et al., 2009; Wu et al., 2001). However, none of them has been shown to regulate *C. elegans* cell cycle progression. Prior genetic studies reported that EGL-44 and EGL-46 (a homolog of human insulinoma-associated protein) control the fate of the touch cell FLP and that EGL-46 is essential for cell cycle exit in Q.ap and Q.paa cells (Wu et al., 2001), but the function of EGL-44/Scalloped in *C. elegans* neuroblast proliferation remains unclear.

Neuronal differentiation involves numerous cell type-specific transcriptional regulatory cascades that determine neuronal fate (Hobert, 2011). A LIM domain TF, MEC-3, positively regulates the expression of mechanosensory genes in one of three Q cell progenies (Way and Chalfie, 1988). Equally intriguing is the inhibition of the touch fate in non-mechanosensory neurons. The *C. elegans* C2H2-type zinc-finger TF PAG-3 is the homolog of the *Drosophila* Senseless proteins and represses touch neuron-specific genes in BDU interneurons (Cameron et al., 2002; Jia et al., 1996; Jia et al., 1997). However, little is known about the repression of the touch fate in Q cell progenies that do not function as the mechanosensory neuron.

This study performed large-scale forward genetic screens, through which we identified three evolutionarily conserved TFs

essential for Q neuroblast lineage progression. Using live cell imaging, genetic and biochemical approaches, we showed that they form three transcriptional regulatory pathways that function sequentially to ensure proper asymmetric cell division, cell cycle exit and cell fate determination in Q neuroblast development.

MATERIALS AND METHODS

C. elegans strains, genetics and DNA manipulations
C. elegans strains were raised on NGM plates seeded with the *Escherichia coli* strain OP50 at 20°C. Strains are listed in supplementary material Table S1. PCR products and plasmid constructs are listed in supplementary material Tables S2 and S3. Integrated P*mec-4::gfp(zdIs5)*, P*gcy-32::mCherry(casIs35)* and P*gcy-32::gfp(casIs36)* transgenes were used to visualize Q neuroblast progenies, AVM/PVM and AQR/PQR. EMS mutagenesis was carried out with a single or with two transgenic markers to identify mutations with an ectopic gain or loss of these neurons. We isolated mutant alleles of known genes in Q neuroblast lineage progression; *cnt-2(cas4)*, *pig-1(cas5)* and *unc-86(cas34, cas60, cas61, cas63, cas144, cas148, cas152)*. Unknown mutations were mapped using snip-SNP techniques and complementation testing (for details of mapping see supplementary material Fig. S1A) and candidate genes in these regions were sequenced to identify mutations.

cas27, *cas46* and *cas137* mutations caused an extra AQR-like or PQR-like neuron phenotype, and they were determined to affect a single gene by complementary tests. Snip-SNP mapping located *cas46* mutations between IV: 5.19 and IV: 7.41. Sequencing of the *ham-1* gene in this region revealed nucleotide changes in *cas27* and *cas137* and a deletion in *cas46* (Fig. 1C,D; supplementary material Fig. S1A).

cas3, *cas6*, *cas19*, *cas58* and *cas140* mutations caused one extra AQR-like or PQR-like neuron phenotype. These mutants showed a weak egg-laying defect phenotype and they ectopically expressed P*mec-4::gfp* in one or two FLP cells. Snip-SNP mapping located this gene to II: –0.96 and II: 0.12. We sequenced three *egl* genes in this region and found mutations in *egl-44* (Fig. 1C,D; supplementary material Fig. S1A).

cas16, *cas18*, *cas24*, *cas25*, *cas36* and *cas133* caused one extra AQR-like or PQR-like neuron phenotype. The mutations were localized to V: 0.11 and V: 0.55 where *egl-46* is located. Sequencing revealed a mutation in the *egl-46* coding region of each allele (Fig. 1C,D; supplementary material Fig. S1A).

cas8, *cas10*, *cas11*, *cas12* and *cas22* mutations caused one extra AVM-like or PVM-like neuron and the Egl phenotype with 100% penetrance, and they were determined to affect a single gene by complementary tests. Snip-SNP mapping located this gene between X: −4.93 and X: −4.38. Microinjection of a single fosmid, WRM068bH06, that carries the DNA sequence spanning part of this region partially rescued both the Egl and extra neuron phenotypes. Sequencing results revealed a Q- or W-to-stop codon mutation in *egl-13* of each allele (Fig. 1C,D; supplementary material Fig. S1A).

Four types of mutation occurred in these alleles: (1) nonsense mutations in *egl-46* (*cas16*, *cas18*, *cas24*, *cas25*, *cas26*) and *egl-13* (*cas8*, *cas10*, *cas11*, *csa12*, *cas22*); (2) missense mutations in *ham-1* (*cas27*, *cas137*), *egl-44* (*cas3*, *cas6*, *cas58*, *cas140*) and *egl-46* (*cas133*); (3) a deletion in *ham-1(cas46)* removed the last 381-414 amino acid and 3′UTR; and (4) a substitution of the consensus 5′ donor splice site of intron 2 in *egl-44(cas19)*.

Our screens and those of others repeatedly identified mutations that changed the same nucleotides in *egl-44* and *egl-46*. Arginine 140 in EGL-44 was mutated to glutamine in *cas6*, *n998*, *n1087*, while *cas16* and *cas36* or *cas18* and *cas24* had identical mutations in *egl-46* (glutamine 101 or 168 to a stop codon), although they were isolated from different strains (*cas16* and *cas18* from P*gcy-32::mCherry*, *cas24* and *cas36* from P*mec-4::gfp* and P*gcy-32::mCherry* double markers).

We did not note any obvious difference in penetrance in the QL and QR lineages of *ham-1*, *egl-44* or *egl-46* mutants. In *egl-13* mutants, the QL and QR lineages had an identical phenotype but with different penetrance, and their data were distinguished (Fig. 6E,F).

We confirmed that these mutants were correctly cloned. All of the canonical alleles of these genes have the same phenotypes as our newly isolated mutant alleles (supplementary material Fig. S1B). GFP- or mCherry-tagged translational fusion constructs of these genes successfully rescued the corresponding mutant phenotypes (supplementary material Fig. S1C).

Live cell imaging
C. elegans L1 larvae were anesthetized with 0.1 mM levamisole (Sigma) in M9 buffer, mounted on 3% agarose pads, and maintained at 20°C. Our imaging system includes an Axio Observer Z1 microscope (Carl Zeiss MicroImaging) equipped with a 100×, 1.45 N.A. objective, an EM CCD camera (Andor iXon+ DU-897D-C00-#BV-500), and the 488-nm and 568-nm lines of a Sapphire CW CDRH USB laser system or an argon and krypton laser attached to a spinning disk confocal scan head (Yokogawa CSU-X1 Spinning Disk Unit). Time-lapse images were acquired with exposure time of 300 mseconds every 30 or 60 seconds by Focus Image software (developed by Mr Xiang Zhang at the Institute of Biophysics, Chinese Academy of Sciences). We used ImageJ software (NIH) to process images. In all images shown, the anterior of Q cells or *C. elegans* is to the left.

Quantification and statistical analysis
Quantification of spindle position and daughter cell size ratio followed our published protocol (Ou et al., 2010). Spindle positioning was quantified by the ratio of the distance of the anterior and posterior centrosomes to the anterior and posterior cell poles (Pa, Pp). Daughter cell size ratio was calculated by Q.aa/Q.ap or Q.pp/Q.pa. Quantification of GFP fluorescence intensity of PIG-1::GFP in wild type (WT) and mutants followed our published methods (Ou and Vale, 2009). The fluorescence intensity of PIG-1 was calculated as fluorescence divided by area using ImageJ. Student's *t*-test or χ^2 analysis was used to examine statistical differences in daughter Q cell size ratio or extra neuron phenotypes in WT and mutants.

HAM-1 binding peak display
Integrated Genome Browser 6.7.3 was used to analyze HAM-1 binding peaks at the *pig-1* promoter. The CHIP-Seq data were downloaded from the modENCODE consortium (www.modencode.org).

Yeast two-hybrid analysis
Sequences encoding EGL-44 and EGL-46 full-length proteins or truncations were cloned into a DNA activation domain (AD) vector (pGADT7, Clontech) and a binding domain (BD) vector (pGBKT7, Clontech) by the in-fusion cloning technique. Plasmids were verified by DNA sequencing. The resulting AD and BD constructs were transformed into the yeast strain AH109 using the Yeastmaker Yeast Transformation System 2 (Clontech). Transformants carrying both AD and BD vectors were initially selected on synthetic complete agar –Leu –Trp medium. To screen protein-protein interaction, a single clone was streaked on the interaction selection media (synthetic complete agar –Leu –Trp –Ade –His) to score growth.

GST fusion protein pull-down assay
E. coli BL21 (DE3) was used to express GST, GST-EGL-44 or His-EGL-46 with induction by 0.3 mM IPTG for 12 hours at 16°C. Bacterial culture was collected and disrupted in lysis buffer (PBS pH 7.32, with 140 mM NaCl, 2.7 mM KCl, 10 mM Na_2HPO_4 and 1.8 mM KH_2PO_4) using a microfluidizer. Bacterial lysate containing His-EGL-46 was incubated with GST lysate or GST-EGL-44 for 30 minutes at 4°C, and glutathione-agarose beads 4B (GE Healthcare) were added to immobilize GST or GST-EGL-44 for another hour at 4°C. The beads were washed three times with PBS. The bound proteins were eluted with elution buffer (10 mM reduced glutathione in PBS) and the eluents were subjected to western blotting with anti-His and anti-GST antibodies (Zhonghan Golden Bridge).

RESULTS
Identification of three evolutionarily conserved transcription factors essential for Q neuroblast lineage progression
To identify factors that control Q neuroblast lineage progression, we carried out GFP- and mCherry-based genetic screens. We used
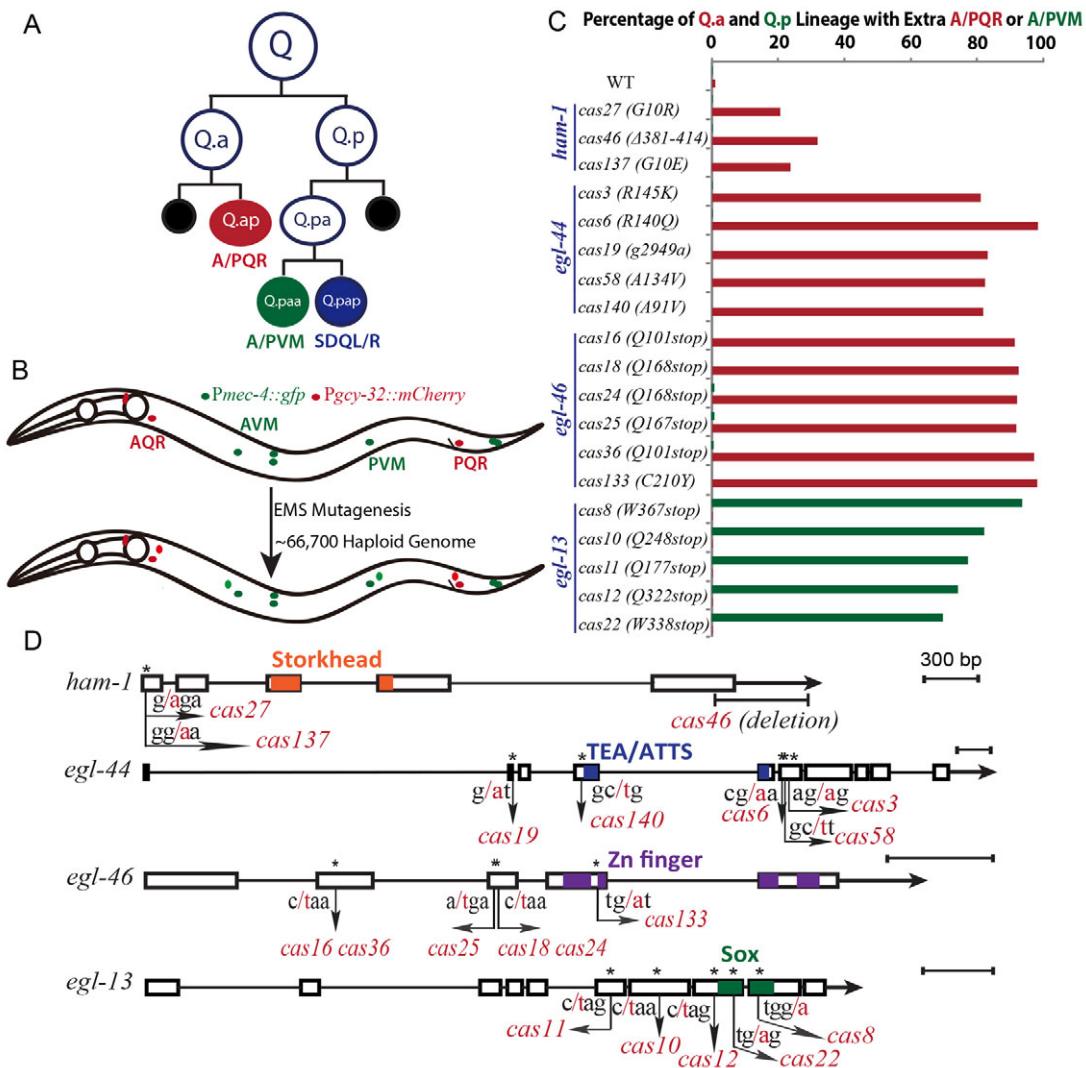
Fig. 1. Three transcription factors regulate *C. elegans* Q neuroblast lineage progression. (**A**) Q neuroblasts undergo asymmetric cell divisions to generate three distinct neurons. On the left side of the animal, QL generates PQR, PVM and SDQL; and on the right QR generates AQR, AVM and SDQR. PQR and AQR (red) sense oxygen, PVM and AVM (green) are mechanosensory neurons, and SDQL and SDQR (blue) are interneurons. (**B**) Genetic screens isolated mutations with extra neurons from Q cell lineages. P*mec-4::gfp* marks AVM and PVM (green) and P*gcy-32::mCherry* labels AQR and PQR (red). See text for further details of the screen. (**C**) Percentages of extra AVM/PVM (green) or AQR/PQR (red) in mutants. Mutations altered *ham-1*, *egl-44*, *egl-46* and *egl-13* (see Materials and methods). n=127-194. (**D**) Gene structures. The genomic region corresponding to the largest unspliced RNA of each isolated gene is indicated; boxes represent exons, solid lines represent introns. Coding regions of conserved domains Storkhead, TEA/ATTS, zinc-finger and Sox are in orange, blue, purple and green, respectively. Nucleotide substitution or deletion mutations are indicated. Asterisks indicate mutation loci.

a mechanosensory neuron-specific reporter construct (P*mec-4::gfp*) and an oxygen sensory neuron-specific reporter construct (P*gcy-32::mCherry*) to isolate mutations that alter the numbers of both neuronal types (Fig. 1B). The *mec-4* promoter drives GFP expression in six mechanosensory neurons, two of which, AVM and PVM (A/PVM), are derived from Q.p asymmetric divisions. The *gcy-32* promoter drives mCherry expression in four oxygen sensory neurons, two of which, AQR and PQR (A/PQR), are produced by the Q.a lineage. Genetic screens using P*mec-4::gfp* have been carried out previously (Cordes et al., 2006; Singhvi et al., 2011); however, screens based on P*gcy-32::mCherry* that are likely to uncover specific factors for Q.a asymmetric division have not been reported. We generated a double-fluorescence labeling strain in which four Q neuroblast progenies can be visualized, and we screened for mutants with an ectopic gain or loss of these neurons

(see Materials and methods) (Fig. 1B). After examining 66,700 haploid genomes treated by ethyl methane sulfonate (EMS), we isolated over 50 mutants with abnormal neuron numbers, including mutant alleles of four genes, *cnt-2*, *egl-46*, *pig-1* and *unc-86*, known to regulate Q cell development (Chalfie et al., 1981; Cordes et al., 2006; Singhvi et al., 2011; Wu et al., 2001).

We identified 13 mutants that did not map to the known loci. Using genetic techniques, we showed that these mutants caused molecular lesions in three evolutionarily conserved TFs (Fig. 1C,D; supplementary material Fig. S1, Fig. S2A; see Materials and methods; BLAST E-values range from $6.5e^{-21}$ to $2.7e^{-71}$): HAM-1 is a homolog of human storkhead box 1 (STOX1) (Frank et al., 2005); EGL-44 is a homolog of human transcriptional enhancer factor TEF5 (TEAD3) (Wu et al., 2001); and EGL-13 is a homolog of the human TF SOX5 (Hanna-Rose and Han, 1999). The functions

of these TFs in neuroblast lineage progression are not well understood. Our study addresses the interaction between EGL-44 and EGL-46, and we isolated six alleles of *egl-46* (Fig. 1C,D).

We next used live cell imaging analysis to determine which cellular processes were defective in these mutants. Among existing mutants, we focused on *ham-1(cas46)*, *egl-44(cas6)*, *egl-46(cas36)* and *egl-13(cas11)* because these alleles include a deletion (*cas46*), the most severe extra neuron phenotype (*cas6*), or the earliest stop codon (*cas36* and *cas11*).

HAM-1 regulates spindle positioning and myosin polarization

HAM-1 was previously shown to control *C. elegans* embryonic but not larval neuroblast asymmetric cell divisions (Frank et al., 2005; Guenther and Garriga, 1996). Although human STOX1/HAM-1 is abundantly expressed in the brain (van Dijk et al., 2010), its neuronal function is largely unknown. We confirmed that Q.p development is independent of *ham-1* as no extra A/PVM were generated in *ham-1* mutants (Fig. 1C). However, *ham-1* mutants generated extra A/PQR neurons (Fig. 1C), indicating that HAM-1 specifically regulates Q.a development.

We studied Q cell asymmetric divisions in *ham-1* and other TF mutants by visualizing the dynamics of the GFP-tagged centrosome, mCherry-labeled chromosome and plasma membrane. We found that only Q.a asymmetric division was defective in *ham-1* mutants (Fig. 2A,E). In WT animals, Q.a positioned its spindle in the cell center, and an anterior accumulation of myosin during cytokinesis was the likely cause of the generation of a small Q.aa and a large Q.ap (Fig. 2A,C) (Ou et al., 2010). In *ham-1* mutants, 62% of QR.a (*n*=13) properly positioned their spindles, but myosin was evenly

distributed in the contractile ring, producing two equal daughter cells; for the remaining 38% of QR.a, the spindle was shifted towards the posterior and myosin symmetrically distributed, producing a large QR.aa and a small QR.ap (Fig. 2A-D; supplementary material Fig. S2B,C).

HAM-1 contains a predicted winged helix DNA-binding motif (Fig. 1D), suggesting that it might function as a TF inside the nucleus. However, prior immunofluorescence studies reported that HAM-1 is asymmetrically localized on the cortex in neuroblasts (Frank et al., 2005; Guenther and Garriga, 1996). We examined the expression and localization of HAM-1 in Q cells using a GFP reporter. The modENCODE consortium constructed an integrant line expressing a GFP-tagged HAM-1 protein under the control of the *ham-1* promoter (P*ham-1*). The P*ham-1::ham-1::gfp* transgene was functional as it reduced the extra A/PQR phenotype from 31% (*n*=196) to 9% (*n*=203) in *ham-1* mutants (supplementary material Fig. S1C). By quantifying daughter cell size asymmetry, we found that the transgene partially rescued the asymmetric cell division defects in *ham-1* mutants (*P*<0.01, Student's *t*-test; the distribution of the raw data in shown in supplementary material Fig. S1D), which correlated with the partial rescue of the extra neuron phenotype. Using this reporter, HAM-1::GFP fluorescence was visible in both Q.a and Q.p as well as in their neighboring cells (supplementary material Movie 1). Time-lapse imaging analysis showed that HAM-1::GFP was restricted to interphase nuclei as with other TFs (e.g. EGL-44, EGL-46 and EGL-13, supplementary material Fig. S3B) and that HAM-1::GFP was evenly distributed in the cytoplasm of dividing Q.a (*n*=14) and Q.p (*n*=10) cells (Fig. 3A; supplementary material Movie 1). The dynamic distribution of HAM-1 suggested that it might function as a TF in Q cells.
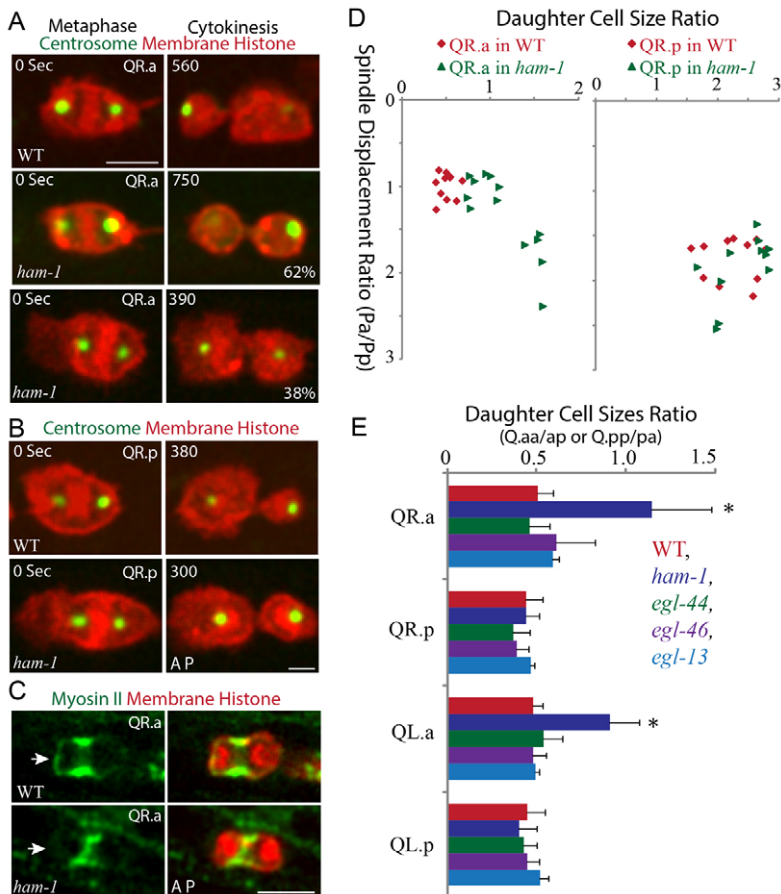

Fig. 2. Q cell asymmetric divisions in *ham-1* mutants.
(**A,B**) Still images show QR.a (A) and QR.p (B) spindle positioning and daughter cell sizes in the WT (top) and *ham-1* mutant (middle/bottom). Centrosomes (green) were marked by GFP-tagged centrosome protein CMD-1; plasma membrane and chromosomes (red) were labeled by mCherry fused with a myristoylation signal and histone (HIS-24). Time is in seconds. (**C**) Myosin II (GFP-tagged NMY-2 in green) distribution in WT (top) and *ham-1* mutant (bottom). Arrows point to the anterior of QR.a. Further frames are shown in supplementary material Fig. S2B,C.
(**D**) Relationship between spindle positioning and daughter cell size ratio of QR.a (left) and QR.p (right) cells in WT (red) and *ham-1* mutants (green). (**E**) Daughter cell size ratio in WT and TF mutants. **P*<0.005, Student's *t*-test; *n*=10-17; error bars indicate s.d. AP indicates that anterior is to left. Scale bars: 5 μm.
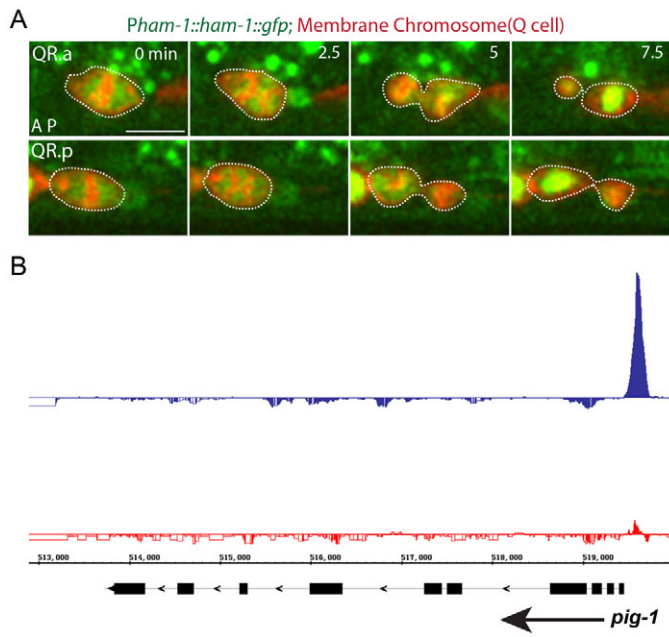
Fig. 3. HAM-1 localizes in the Q cell nucleus and is associated with the *pig-1* promoter. (A) HAM-1::GFP dynamics in QR.a and QR.p asymmetric divisions. Metaphase (0 minutes), anaphase (2.5 minutes), cytokinesis (5 minutes) and post-division (7.5 minutes). Dotted lines indicate Q cell periphery. Scale bar: 5 μm. **(B)** Chip-Seq data show that HAM-1 is associated with the promoter (blue) of the *pig-1* gene. Input (the negative control in Chip-Seq) is in red. The *pig-1* gene model is in black. The arrow indicates the direction of transcription.

HAM-1 promotes *pig-1* expression for Q cell asymmetric division

To understand how HAM-1 regulates Q.a asymmetric division, we searched for its transcriptional regulatory target. The modENCODE consortium used chromatin immunoprecipitation coupled with high-throughput DNA sequencing (CHIP-seq) to search for the genome-wide binding sites of HAM-1 in *C. elegans* L1 larvae. From the original datasets, we uncovered that HAM-1 is bound to the promoter region of the *pig-1* gene (−266 to –42 bp relative to the ATG; Fig. 3B). PIG-1 is a member of the conserved PAR-1/Kin1/SAD-1 family of serine/threonine kinases that regulate polarity and asymmetric cell division, and the inhibition of *pig-1* phenocopied the *ham-1* extra neuron phenotype in the Q.a cell (Cordes et al., 2006). Our previous imaging analysis showed that myosin polarization during Q.a cytokinesis was disrupted in *pig-1* mutants (Ou et al., 2010). Furthermore, the prior genetic analysis suggested that *pig-1* acted downstream of *ham-1* (Cordes et al., 2006). Thus, *pig-1* is a likely functional target of HAM-1.

We first examined whether HAM-1 promoted *pig-1* expression in Q cells. We constructed a strain expressing P*pig-1::pig-1::gfp* and showed that the transgene was functional because it reduced extra A/PQR neurons in *pig-1(gm344)* mutants from 19% (*n*=154) to 2% (*n*=174). After crossing the transgene into *ham-1* mutants, we compared the expression of P*pig-1::pig-1::gfp* in WT and *ham-1* mutants. The PIG-1::GFP fluorescence was visible in all the WT Q.a cells (*n*=18), but was significantly reduced in *ham-1* mutants (Fig. 4A,B). PIG-1::GFP fluorescence did not change in neighboring seam cells of *ham-1* mutants (Fig. 4A,B, asterisks), suggesting that we could use PIG-1::GFP in seam cells as a fiduciary marker to further quantify PIG-1::GFP changes in Q cells. We measured the fluorescence intensity ratio between Q.a and seam cells within the same animal. PIG-1::GFP in Q.a was 3.3-fold brighter than that of the seam cell (*n*=18) in WT animals, but this intensity ratio was reduced to 1.4 in *ham-1* mutants (*n*=24; *P*<0.005, Student's *t*-test) (Fig. 4C). Thus, HAM-1 positively regulates *pig-1* expression in Q.a.

To study the significance of the HAM-1 binding site in the *pig-1* promoter, we deleted it from a functional P*pig-1::pig-1::gfp* plasmid. This completely abolished *pig-1::gfp* expression in the Q.a cell (100%, four independent transgenic lines, 10-15 worms were examined from each line; Fig. 4D, right). As a negative control, the deletion of another region in the *pig-1* promoter (−633 to –407 from
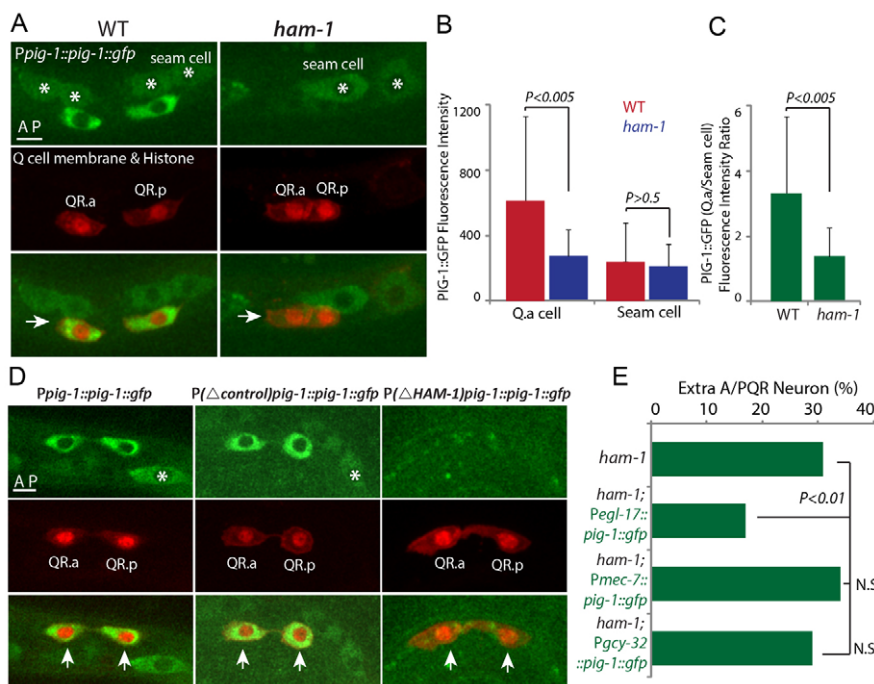

Fig. 4. HAM-1 promotes *pig-1* expression for Q cell asymmetric division. (A) Still images show PIG-1::GFP fluorescence in WT (left) and *ham-1* mutant (right). PIG-1::GFP was expressed by the *pig-1* promoter (green, top). Q cell plasma membrane and chromosomes were marked with mCherry (red, middle). In the merged images (bottom) arrows point to the Q.a cell. Asterisks (A,D) indicate seam cells. **(B)** Quantification of PIG-1::GFP fluorescence intensities in the Q.a cell or seam cell of WT or *ham-1* mutants. **(C)** Quantification of the PIG-1::GFP fluorescence intensity ratio between the Q.a cell and seam cell in WT and *ham-1* mutants. (B,C) *n*=18-24; error bars indicate s.d. Student's *t*-tests were used. **(D)** PIG-1::GFP expression under the control of the *pig-1* WT promoter (left) or with the deletion of a negative control fragment (middle) or the HAM-1 binding site (right). PIG-1::GFP (green, top), Q cell (mCherry, red, middle) and merge (bottom), in which arrows point to Q.a and Q.p. **(E)** The extra A/PQR neuron phenotype in *ham-1* mutants and in *ham-1* animals that expressed *pig-1::gfp* via HAM-1-independent promoters. χ² analysis was used; N.S., not significant. *n*=52-154. AP indicates that anterior is to left. Scale bars: 5 μm.

the ATG) did not change PIG-1::GFP fluorescence in three independent transgenic lines (Fig. 4D, middle). Thus, the HAM-1 binding site in the *pig-1* promoter is essential for *pig-1* expression.

To validate the role of HAM-1 in the transcriptional regulation of *pig-1* further, we examined whether the expression of *pig-1* by HAM-1-independent promoters, such as P*egl-17*, P*gcy-32* or P*mec-7*, could rescue the defects in Q.a asymmetric division in *ham-1* mutants. We introduced a transgene that expresses *pig-1::gfp* under the control of P*egl-17*, a promoter active throughout Q cell development, into *ham-1* mutants. By quantifying A/PQR neuron numbers, we found that the P*egl-17::pig-1::gfp* transgene partially reduced the occurrence of extra A/PQR from 31% to 17% in *ham-1* mutants (*P*<0.01 by χ^2 analysis; Fig. 4E), suggesting that bypassing HAM-1 regulation of the *pig-1* promoter partially rescued asymmetric division defects in *ham-1* mutants. The rescue depended on the developmental stage. We expressed *pig-1::gfp* under the P*gcy-32* or P*mec-7* promoter, neither of which is active until Q cell differentiation, and did not observe any rescue of the extra A/PQR phenotype (Fig. 4E).

Taken together, HAM-1 positively regulates *pig-1* expression during Q.a asymmetric division, possibly through the *pig-1* promoter region.

EGL-44 and EGL-46 bind to each other and control cell cycle exit

Prior studies reported that EGL-44 and EGL-46 repress touch cell fate in FLP cells and that EGL-46 regulates cell cycle exit in Q cell lineages (Desai and Horvitz, 1989; Wu et al., 2001). However, whether EGL-44 is involved in cell cycle regulation has not been determined. We uncovered multiple alleles of *egl-44* and *egl-46* with the ectopic gain of A/PQR neurons (Fig. 1C,D). Time-lapse recording showed that EGL-44 controls cell cycle exit in Q.ap and Q.paa cells (Fig. 5A; supplementary material Movies 2, 3). Using QR.ap as an example, QR.ap differentiated into AQR in WT animals (Fig. 5A); however, QR.ap had one extra round of division at 158±19 minutes after birth in *egl-44* mutants (*n*=9) or 158±34 minutes after birth in *egl-46* animals (*n*=6) (Fig. 5A). Both QR.ap daughter cells differentiated into neurons expressing oxygen sensory neuron-specific genes, resulting in extra A/PQR in *egl-44* or *egl-46* mutants (Fig. 1C, Fig. 5A; supplementary material Movies 2, 3).

We next examined the expression pattern of *egl-44* and *egl-46*. *egl-44* was expressed throughout the Q cell lineage, whereas *egl-46* was only expressed in a subset of this lineage. Initially, *egl-46* was not expressed in the Q neuroblast, and in the Q.a lineage it started to be expressed in the Q.a cell, whereas in the Q.p lineage its expression was restricted to Q.paa and was absent from Q.pap (supplementary material Fig. S3A) (Wu et al., 2001). Cell cycle exit in *egl-46* mutants is only defective in Q.ap or Q.paa cells, indicating that EGL-46 is specifically expressed in cells where it is essential.

Since *egl-44* and *egl-46* mutants have the same phenotype in terms of cell cycle regulation and FLP cell differentiation, we examined whether they physically bind to each other. Yeast two-hybrid assays detected the interaction between full-length EGL-44 and EGL-46 (Fig. 5B,C). We narrowed down the minimal regions for their association; the EGL-44 N-terminal fragment, including the TEAD domain, was sufficient to bind to the EGL-46 C-terminal fragment, including the zinc-finger domain (Fig. 5B,C). We used
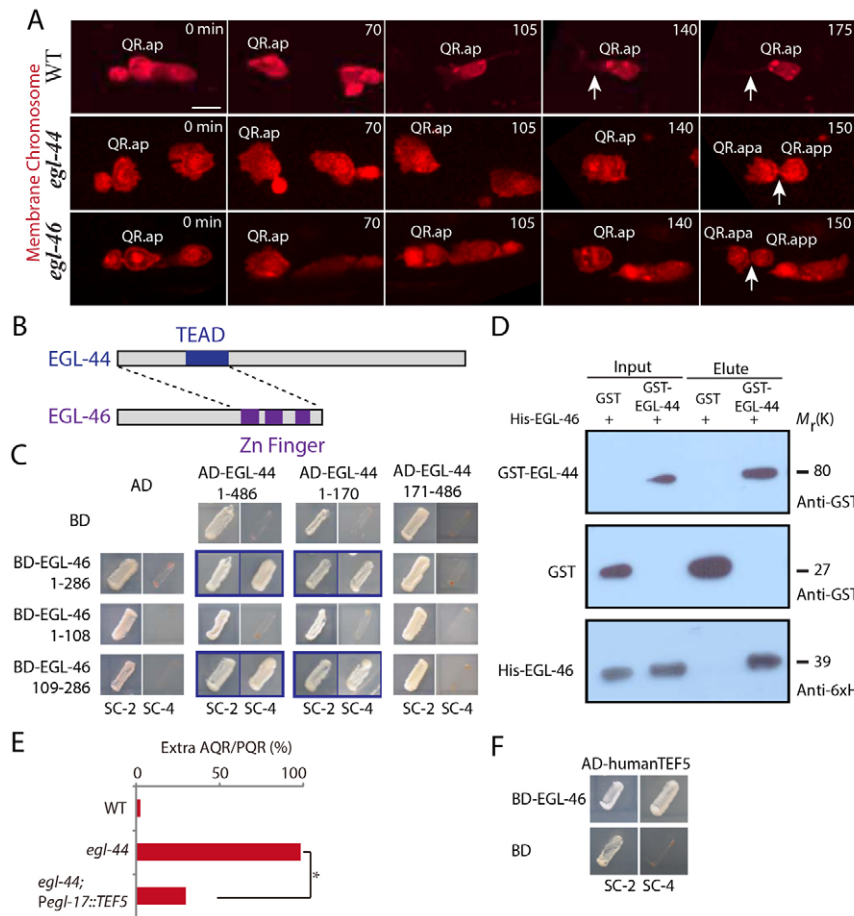

Fig. 5. EGL-44 binds to EGL-46 and both control Q cell cycle exit. (**A**) QR.ap differentiated in WT (upper) or underwent one extra round of division in *egl-44* (middle) or *egl-46* (lower) mutants. Arrows indicate the QR.ap dendrite in WT (140, 175 minutes) or an extra round of division of QR.ap in *egl-44* and *egl-46* (150 minutes). Time is in minutes. Scale bar: 5 μm. (**B**) Overview of EGL-44 and EGL-46 interaction. Dashed lines indicate interaction domains. (**C**) Interaction between EGL-44 and EGL-46 in the yeast two-hybrid system. Yeast transformants expressing both Gal4 DNA-binding domain (BD)-EGL-46 full-length (1-286) or N(1-108) or C(109-286) terminal truncation fusions and the Gal4 transcription activation domain (AD)-EGL-44 full-length (1-486) or N(1-170) or C(171-486) terminal truncation fusions were streaked on synthetic complete medium lacking Trp and Leu (SC-2, left) or lacking Trp, Leu, His and Ade (SC-4, right). Growth on SC-4 indicated interaction between two tested fusion proteins. (**D**) Interaction between EGL-44 and EGL-46 in a GST fusion protein pull-down assay. GST-EGL-44, His-EGL-46 and the control GST were used in the binding reactions. Shown are detections of GST-EGL-44 (top), GST (middle) and His-EGL-46 (bottom) in western blots. (**E**) Q cell-specific expression of the human EGL-44 homolog TEF5 (TEAD3) under the control of the *egl-17* promoter rescued the extra AQR/PQR phenotype of the *egl-44* mutant. *P<0.005, Student's *t*-test; *n*=22-35. (**F**) Yeast two-hybrid assay of *C. elegans* EGL-46 and human TEF5.

protein pull-down assays with glutathione *S*-transferase (GST) fusion proteins to show that His-tagged EGL-46 bound to GST-tagged EGL-44 but not to the GST protein alone (Fig. 5D). Thus, EGL-44 and EGL-46 might function in a transcriptional regulatory protein complex to promote cell cycle exit.
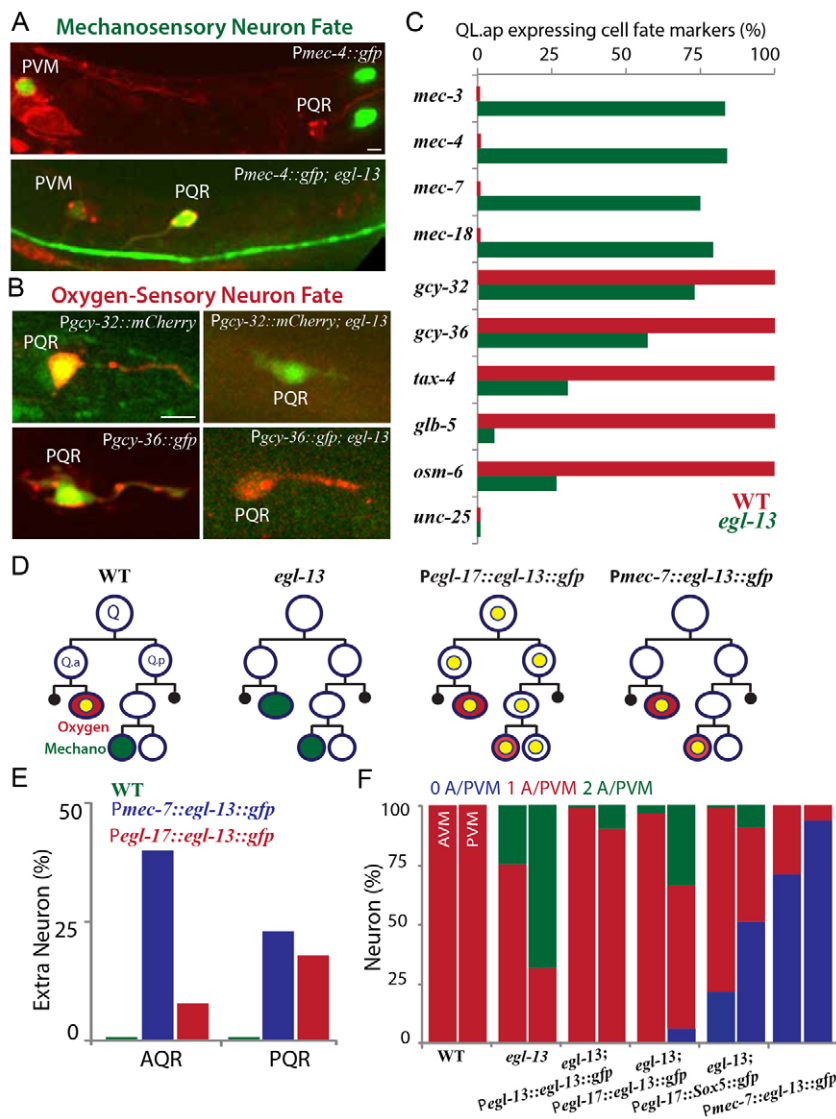
EGL-13 determines neuronal fate

EGL-13 belongs to an SRY box (Sox)-containing gene family (Fig. 1D). EGL-13 was initially identified from defects in the connection between the uterus and the vulva in *C. elegans* (Cinar et al., 2003; Hanna-Rose and Han, 1999). SOX5 and SOX6, which are vertebrate homologs of EGL-13, are involved in chondrogenesis and in the cell cycle progression of neural progenitors in the chick spinal cord; however, little is known about their function in neural fate determination. We found that *egl-13* mutants generated extra A/PVM (Fig. 1C) but lost neurons in the Q.a lineage (AQR or PQR was absent in 22% or 42%, respectively, of *egl-13* animals; *n*=77).

We examined the neuronal differentiation of Q.ap cells in *egl-13* mutants. For example, QL.ap normally differentiates to PQR by expressing oxygen sensory neuron-specific genes such as P*gcy-32::mCherry*. In *egl-13* mutants, QL.ap did not express P*gcy-32::mCherry* but ectopically expressed P*mec-4::gfp*, a marker characteristic of mechanosensory neurons (Fig. 6A,B), indicating

that QL.ap was likely to be programmed from an oxygen sensory neuron to a touch neuron. Consistently, QL.ap expressed both P*gcy-32::mCherry* and P*mec-4::gfp* in 53.3% of *egl-13* mutants (*n*=45), which might be intermediates of both neuronal fates. We examined additional neuronal markers to confirm the neuronal fate transition. In A/PVM, *mec-3*, *mec-4*, *mec-7* and *mec-18* encode touch neuron-specific TF, channel protein, tubulin and CoA synthetase, respectively. No PQR expressed these genes in WT animals, whereas 75-88% of PQR neurons ectopically expressed them in *egl-13* mutants (Fig. 6C; supplementary material Fig. S4A). In A/PQR, *gcy-32*, *gcy-36*, *tax-4* and *glb-5* encode membrane receptors or signaling molecules specifically for oxygen sensation. A/PQR neurons are ciliated, and the ciliogenesis depends on the action of intraflagellar transport proteins (e.g. OSM-6). We compared the expression of A/PQR-specific genes in WT and *egl-13* animals. All the WT PQR neurons expressed these markers, but PQR neurons expressed them in 6-73% of *egl-13* mutants (Fig. 6C; supplementary material Fig. S4B). EGL-13 thus determines the neuronal fate in Q cell lineages.

MEC-3 is a key TF for *mec* gene expression, and the ectopic expression of *mec* genes in Q.ap of *egl-13* mutants requires MEC-3 because Q cell progenies do not express *mec* genes in *egl-13; mec-3* double mutants (supplementary material Fig. S4C, right). We also

Fig. 6. EGL-13 determines neuronal fate.
(**A**) Mechanosensory neurons were marked by P*mec-4::gfp* in WT and *egl-13* mutants. Q cells were labeled by mCherry fused with a myristoylation signal and histone. (**B**) Oxygen sensory neurons were marked by P*gcy-32::mCherry* (top) or P*gcy-36::gfp* (bottom) in WT and *egl-13* mutants. Q cells were marked by cytosolic GFP (top) or were labeled as in A (bottom). (**C**) Quantification of QL.ap/PQR expression of mechanosensory and oxygen sensory markers in WT (red) and *egl-13* mutant (green). *n*=12-33. The *unc-25* gene was used as a control to show that not every neuronal fate was changed in *egl-13* mutants. (**D**) Schematics showing that ectopic expression of *egl-13* in AVM and PVM changed their neuronal fates. In WT animals, the Q.ap cell specifically expressed *egl-13* (yellow circle) and differentiated into oxygen sensory neurons (red). The Q.ap cell lost the properties of an oxygen sensory neuron but acquired the fate of a mechanosensory neuron (green) in *egl-13* mutants. The ectopic expression of *egl-13* caused the abnormal gain of the oxygen sensory property and the loss of the mechanosensory property in A/PVM. (**E**) Percentage of extra A/PQR neurons that ectopically expressed P*gcy-32::mCherry* in *egl-13*-related genetic backgrounds. *n*=66-102. (**F**) Quantification of P*mec-4::gfp* expression in AVM (left) and PVM (right) in different *egl-13*-related genetic backgrounds. No (blue), one (red) or two (green) neurons expressed P*mec-4::gfp*. *n*=45-98.

found that *egl-13* single mutants and *egl-13; mec-3* double mutants did not differ in the loss of A/PQR (supplementary material Fig. S4C), indicating that the loss of A/PQR in *egl-13* worms does not require *mec-3*. EGL-13 might repress the touch fate by inhibiting *mec-3* and support A/PQR fate independently of *mec-3*.

EGL-13 is sufficient for neuronal fate determination

We studied the expression pattern of *egl-13* in Q cell lineages. Using a transcriptional fusion reporter with *gfp*, we found that *egl-13* started to be expressed after Q.a divisions and that GFP fluorescence reached the maximum level in Q.ap upon differentiation (supplementary material Fig. S4D, Movie 4). By contrast, the GFP signal was barely detected in the Q.p lineage, and the mCherry fluorescence in Q cells did not change during Q cell development (supplementary material Fig. S4D, Movie 4). *egl-13* was continuously expressed in A/PQR during larval development (supplementary material Fig. S3C, e.g. L3 larval stage), indicating that EGL-13 can be involved in neuronal fate initiation and maintenance.

To address whether EGL-13 is sufficient for neuronal fate determination, we ectopically expressed it in A/PVM, where EGL-13 is normally absent. Two promoters were used for EGL-13::GFP expression; P*egl-17* was active throughout the entire Q cell lineage, whereas P*mec-7* was only switched on in A/PVM upon differentiation (Fig. 6D). Both transgenes could induce ectopic A/PQR neurons (Fig. 6E). For instance, extra AQR neurons were produced in 40% of transgenic animals expressing P*mec-7::egl-13::gfp*. Since the P*mec-7* promoter was stronger than P*egl-17* during differentiation, P*mec-7::egl-13::gfp* induced a higher percentage of extra A/PQR neurons than P*egl-17::egl-13::gfp* (Fig. 6E). In addition, both transgenes inhibited the touch fate in A/PVM. In WT animals, 100% of A/PVM expressed the P*mec-4::gfp* reporter. The P*mec-7::egl-13::gfp* transgene significantly reduced the number of GFP-positive A/PVM, and 71% of AVM and 94% of PVM lost their GFP fluorescence from P*mec-4::gfp* (Fig. 6F). The P*egl-17::egl-13::gfp* transgene also inhibited the PVM fate (Fig. 6F).

Collectively, these data demonstrated that *egl-13* is necessary and sufficient to determine the neuronal fate in the Q cell lineage.

The additive action of *ham-1, egl-44/egl-46* and *egl-13* in Q cell development

We performed double-mutant analysis to investigate interactions between the TFs. Single-mutant analysis showed that *ham-1* controlled Q.a asymmetric division, whereas *egl-44/egl-46* regulated Q.ap cell cycle exit (supplementary material Fig. S5A). We found that 7.8% of *ham-1; egl-44* (*n*=51) and 20.5% of *ham-1; egl-46* (*n*=34) double mutants generated four PQR-like neurons (supplementary material Fig. S5B), indicating that the disruption of asymmetric cell division in *ham-1* and of cell cycle exit in *egl-44/46* could be additive. EGL-13 determined the neuronal property of Q.ap (supplementary material Fig. S5A). We found that 12% of *ham-1; egl-13* double mutants (*n*=80) produced three PVM-like neurons, two of which could arise from additive defects in Q.a asymmetric division of *ham-1* and of daughter cell differentiation in *egl-13* (supplementary material Fig. S5B). Similarly, 4.2% of *egl-44; egl-13* double mutants (*n*=120) generated three PVM-like neurons, probably resulting from the failures of QL.ap cell cycle exit in *egl-44* and of QL.ap daughter cell differentiation in *egl-13* (supplementary material Fig. S5B). The double-mutant analysis suggested that three transcriptional regulatory pathways additively control Q neuroblast development.

Evolutionarily conserved functions of EGL-44 and EGL-13

To explore the conserved function of the TFs, we expressed human TEF5/EGL-44 and SOX5/EGL-13 in *C. elegans egl-44* and *egl-13* mutants, respectively. The extra A/PQR phenotype was reduced by TEF5 from 92% to 30% in *egl-44* worms (Fig. 5E) and the extra A/PVM phenotype was also reduced by SOX5 in *egl-13* mutants (Fig. 6F). The ectopic expression of SOX5 in mechanosensory neurons inhibited the touch fate of A/PVM (Fig. 6F). Furthermore, the yeast two-hybrid assay detected the direct interaction of human TEF5 and *C. elegans* EGL-46 (Fig. 5F). These results suggest that human TEF5 and SOX5 could be functional homologs of *C. elegans* EGL-44 and EGL-13.

DISCUSSION

This study identified three transcriptional regulatory pathways that sequentially control asymmetric cell divisions, cell cycle exit and differentiation in *C. elegans* Q neuroblast development (supplementary material Fig. S5A). We suggest that homologs of these TFs might have conserved functions in vertebrate neural development.

Our work first demonstrated that HAM-1 specifically controls Q.a but not Q.p division, providing molecular insight into their distinct cell division patterns. We propose that HAM-1 and PIG-1 regulate myosin polarization and the asymmetric segregation of cell fate determinants during the Q.a cell division. In *ham-1* or *pig-1* mutants, the Q.a cell divided symmetrically and the equal segregation of neural fate determinants transformed the normally apoptotic daughter cell into its sister cell. Alternatively, HAM-1 and PIG-1 might independently control asymmetric cell divisions and the asymmetric segregation of fate determinants. Consistent with this model, Q.a daughter cell size asymmetry was 100% disrupted in *ham-1* or *pig-1* mutants, but extra A/PQR neurons were generated in only 31% of *ham-1* or 19% of *pig-1* mutants, indicating that daughter cell sizes do not fully specify neuronal fates. To generate extra neurons, the HAM-1/PIG-1 pathway must cooperate with others pathways (e.g. an inhibition of apoptosis) to allow daughter cell survival and differentiation.

pig-1 might act differently in Q.a and Q.p development. Although more ectopic neurons are generated from the Q.p lineage (42% extra A/PVM) than those from the Q.a lineage (19% extra A/PQR) in *pig-1* mutants (Cordes et al., 2006), Q.a and Q.p asymmetric cell divisions are 100% converted to symmetric division in *pig-1* mutants (Ou et al., 2010). These observations are consistent with the notion that PIG-1 may play independent roles in asymmetric cell division and in the asymmetric segregation of fate determinants (Cordes et al., 2006). For neuronal fate determination, PIG-1 might be more essential in the Q.p lineage than in the Q.a lineage, as *pig-1* mutants produce more ectopic A/PVM than ectopic A/PQR. For asymmetric cell division, PIG-1 might be more crucial for Q.a asymmetric division than Q.p division, as the PIG-1 protein level is reduced in both Q.a and Q.p of *ham-1* mutants but only Q.a asymmetric division is altered.

HAM-1 might have different functions in embryonic and postembryonic neuroblast lineages. Immunofluorescence studies reported that HAM-1 is asymmetrically localized on the cortex in embryonic neuroblasts and that it is not expressed in larvae (Frank et al., 2005; Guenther and Garriga, 1996). The absence of HAM-1 signal by immunostaining in larvae might be due to inefficient antibody penetration owing to the thick cuticle of *C. elegans*. Using a functional P*ham-1::ham-1::gfp* strain, we did not detect any asymmetric localization of HAM-1 throughout the Q.a and Q.p cell

cycle (Fig. 3A; supplementary material Movie 1). Furthermore, our CHIP-seq data analysis and functional studies demonstrated that HAM-1 could function as a TF to promote *pig-1* expression in the Q.a cell.

HAM-1 might transcribe other genes for Q.a divisions. In *pig-1* mutants, all the Q.a division was converted into symmetric division. In *ham-1* mutants, 68% of Q.a divided symmetrically, while the other 32% made a large Q.aa and a small Q.ap by completely reversing the polarity (Fig. 2A,D), which might be caused by the loss of other HAM-1 targets than PIG-1. Consistently, the introduction of *pig-1* under the control of the *egl-17* promoter into Q cells only partially reduced the extra A/PQR of *ham-1* mutants (Fig. 4E). It might be that multiple TFs regulate *pig-1* expression, as although deletion of the HAM-1 binding site in the *pig-1* promoter completely abolished *pig-1* expression throughout the entire animal, *pig-1* expression was only reduced in the Q cells of *ham-1* mutants (Fig. 4A-D). *pig-1* expression was reduced in Q.p of *ham-1* mutants but Q.p divisions were normal (Fig. 4A, Fig. 2B,D), suggesting that Q.p division might require less PIG-1 than Q.a division.

This study links *C. elegans* Hippo components to cell cycle regulation. EGL-44, human TEF5 and *Drosophila* Scalloped are homologous TFs, but our work showed that EGL-44 promotes cell cycle exit (Fig. 5A), which is opposite to the function of TEF5 and Scalloped in promoting cell proliferation. Thus, Hippo components might have modulated functions across species. The physical association of EGL-44 and EGL-46 implied that the vertebrate EGL-46 homolog INSM1 might be a previously unknown component in the Hippo signaling pathway. INSM1 plays a pan-neurogenic role in promoting basal progenitor formation in the neocortex (Farkas et al., 2008), and inhibition of INSM1 reduces the radial thickness of the cortical plate, whereas its ectopic expression allows neuroepithelial cells to undergo self-amplification (Farkas et al., 2008), indicating its potential function in cell cycle regulation. The *Drosophila* homolog of EGL-46, Nerfin-1, is expressed in neuroblasts and regulates early axon guidance in the central nervous system (Kuzin et al., 2005; Stivers et al., 2000), but its function in neuroblast divisions has yet to be determined.

Extra A/PQR neurons were generated in *egl-44/egl-46* and *unc-86* mutants. In *egl-44/egl-46* mutants, an extra round of Q.ap cell division gave rise to extra A/PQR neurons. In *unc-86* mutants, extra A/PQR neurons were produced by the reiteration of the Q neuroblast lineage in the Q.p cell (Chalfie et al., 1981). We did not find any changes in *egl-44/egl-46* expression in *unc-86* mutants (supplementary material Fig. S3D). EGL-44/EGL-46 determined the touch fate of FLP neurons (Wu et al., 2001) but not in Q cell lineages (Fig. 5A; supplementary material Fig. S5A), and we found that *egl-13* was expressed in two AQR neurons of *egl-44* mutants (supplementary material Fig. S3E).

Our study has uncovered a novel function of EGL-13/SOX5 family TFs in neuronal fate determination. Vertebrate EGL-13/SOX5 regulates the differentiation of prechondrocytes into chrondroblasts (Smits et al., 2004). In the nervous system, SOX5 controls the timing of cell cycle exit by opposing the activity of Wnt/β-catenin in the chicken spinal cord (Martinez-Morales et al., 2010). Mammalian SOX5 regulates the pace of differentiation of corticofugal neurons by fine-tuning the identity of the various closely related subtypes (Lai et al., 2008). This work has shown that EGL-13 represses the touch fate in non-mechanosensory neurons of the Q cell lineage (Fig. 6). The fate of touch neurons can be inhibited by different transcriptional regulatory mechanisms in different lineages. In *C. elegans pag-3* mutants, the mechanosensory

genes of ALM touch neurons are ectopically expressed in lineally related BDU interneurons (Cameron et al., 2002; Jia et al., 1996; Jia et al., 1997). Taken together, our study demonstrates that three transcriptional regulatory pathways function at distinct development stages to ensure neuroblast lineage progression in *C. elegans*. The identification of additional transcriptional targets will further advance our understanding of neuroblast development.

Author contributions
G.F., P.Y., Y.Y., Y.C., D.T. and G.O. designed experiments; G.F., P.Y., Y.Y., Y.C., D.T., Z.Z., J.L., F.Z., Z.C., X.W. and W.L. performed experiments; G.O. wrote the manuscript.

References
Cabernard, C., Prehoda, K. E. and Doe, C. Q. (2010). A spindle-independent cleavage furrow positioning pathway. *Nature* **467**, 91-94.

Cai, Q., Wang, W., Gao, Y., Yang, Y., Zhu, Z. and Fan, Q. (2009). Ce-wts-1 plays important roles in Caenorhabditis elegans development. *FEBS Lett.* **583**, 3158-3164.

Cameron, S., Clark, S. G., McDermott, J. B., Aamodt, E. and Horvitz, H. R. (2002). PAG-3, a Zn-finger transcription factor, determines neuroblast fate in C. elegans. *Development* **129**, 1763-1774.

Chalfie, M., Horvitz, H. R. and Sulston, J. E. (1981). Mutations that lead to reiterations in the cell lineages of C. elegans. *Cell* **24**, 59-69.

Cinar, H. N., Richards, K. L., Oommen, K. S. and Newman, A. P. (2003). The EGL-13 SOX domain transcription factor affects the uterine pi cell lineages in Caenorhabditis elegans. *Genetics* **165**, 1623-1628.

Cordes, S., Frank, C. A. and Garriga, G. (2006). The C. elegans MELK ortholog PIG-1 regulates cell size asymmetry and daughter cell fate in asymmetric neuroblast divisions. *Development* **133**, 2747-2756.

Desai, C. and Horvitz, H. R. (1989). Caenorhabditis elegans mutants defective in the functioning of the motor neurons responsible for egg laying. *Genetics* **121**, 703-721.

Farkas, L. M., Haffner, C., Giger, T., Khaitovich, P., Nowick, K., Birchmeier, C., Pääbo, S. and Huttner, W. B. (2008). Insulinoma-associated 1 has a panneurogenic role and promotes the generation and expansion of basal progenitors in the developing mouse neocortex. *Neuron* **60**, 40-55.

Frank, C. A., Hawkins, N. C., Guenther, C., Horvitz, H. R. and Garriga, G. (2005). C. elegans HAM-1 positions the cleavage plane and regulates apoptosis in asymmetric neuroblast divisions. *Dev. Biol.* **284**, 301-310.

Gönczy, P. (2008). Mechanisms of asymmetric cell division: flies and worms pave the way. *Nat. Rev. Mol. Cell Biol.* **9**, 355-366.

Guenther, C. and Garriga, G. (1996). Asymmetric distribution of the C. elegans HAM-1 protein in neuroblasts enables daughter cells to adopt distinct fates. *Development* **122**, 3509-3518.

Hanna-Rose, W. and Han, M. (1999). COG-2, a sox domain protein necessary for establishing a functional vulval-uterine connection in Caenorhabditis elegans. *Development* **126**, 169-179.

Hobert, O. (2011). Regulation of terminal differentiation programs in the nervous system. *Annu. Rev. Cell Dev. Biol.* **27**, 681-696.

Hsieh, J. (2012). Orchestrating transcriptional control of adult neurogenesis. *Genes Dev.* **26**, 1010-1021.

Iwasa, H., Maimaiti, S., Kuroyanagi, H., Kawano, S., Inami, T., Ikeda, M., Nakagawa, K. and Hata, Y. (2013). Yes-associated protein homolog, YAP-1, is involved in the thermotolerance and aging in the nematode Caenorhabditis elegans. *Exp. Cell Res.* **319**, 931-945.

Jia, Y., Xie, G. and Aamodt, E. (1996). pag-3, a Caenorhabditis elegans gene involved in touch neuron gene expression and coordinated movement. *Genetics* **142**, 141-147.

Jia, Y., Xie, G., McDermott, J. B. and Aamodt, E. (1997). The C. elegans gene pag-3 is homologous to the zinc finger proto-oncogene gfi-1. *Development* **124**, 2063-2073.

Kang, J., Shin, D., Yu, J. R. and Lee, J. (2009). Lats kinase is involved in the intestinal apical membrane integrity in the nematode Caenorhabditis elegans. *Development* **136**, 2705-2715.

Kuzin, A., Brody, T., Moore, A. W. and Odenwald, W. F. (2005). Nerfin-1 is required for early axon guidance decisions in the developing Drosophila CNS. *Dev. Biol.* **277**, 347-365.

Lai, T., Jabaudon, D., Molyneaux, B. J., Azim, E., Arlotta, P., Menezes, J. R. and Macklis, J. D. (2008). SOX5 controls the sequential generation of distinct corticofugal neuron subtypes. *Neuron* **57**, 232-247.

Martinez-Morales, P. L., Quiroga, A. C., Barbas, J. A. and Morales, A. V. (2010). SOX5 controls cell cycle progression in neural progenitors by interfering with the WNT-beta-catenin pathway. *EMBO Rep.* **11**, 466-472.

Ming, G. L. and Song, H. (2011). Adult neurogenesis in the mammalian brain: significant answers and significant questions. *Neuron* **70**, 687-702.

Ou, G. and Vale, R. D. (2009). Molecular signatures of cell migration in C. elegans Q neuroblasts. *J. Cell Biol.* **185**, 77-85.

Ou, G., Stuurman, N., D'Ambrosio, M. and Vale, R. D. (2010). Polarized myosin produces unequal-size daughters during asymmetric cell division. *Science* **330**, 677-680.

Pan, D. (2010). The hippo signaling pathway in development and cancer. *Dev. Cell* **19**, 491-505.

Singhvi, A., Teuliere, J., Talavera, K., Cordes, S., Ou, G., Vale, R. D., Prasad, B. C., Clark, S. G. and Garriga, G. (2011). The Arf GAP CNT-2 regulates the apoptotic fate in C. elegans asymmetric neuroblast divisions. *Curr. Biol.* **21**, 948-954.

Smits, P., Dy, P., Mitra, S. and Lefebvre, V. (2004). Sox5 and Sox6 are needed to develop and maintain source, columnar, and hypertrophic chondrocytes in the cartilage growth plate. *J. Cell Biol.* **164**, 747-758.

Stivers, C., Brody, T., Kuzin, A. and Odenwald, W. F. (2000). Nerfin-1 and -2, novel Drosophila Zn-finger transcription factor genes expressed in the developing nervous system. *Mech. Dev.* **97**, 205-210.

Sulston, J. E. and Horvitz, H. R. (1977). Post-embryonic cell lineages of the nematode, Caenorhabditis elegans. *Dev. Biol.* **56**, 110-156.

van Dijk, M., van Bezu, J., Poutsma, A., Veerhuis, R., Rozemuller, A. J., Scheper, W., Blankenstein, M. A. and Oudejans, C. B. (2010). The pre-eclampsia gene STOX1 controls a conserved pathway in placenta and brain upregulated in late-onset Alzheimer's disease. *J. Alzheimers Dis.* **19**, 673-679.

Way, J. C. and Chalfie, M. (1988). mec-3, a homeobox-containing gene that specifies differentiation of the touch receptor neurons in C. elegans. *Cell* **54**, 5-16.

Wu, J., Duggan, A. and Chalfie, M. (2001). Inhibition of touch cell fate by egl-44 and egl-46 in C. elegans. *Genes Dev.* **15**, 789-802.

Zhao, C., Deng, W. and Gage, F. H. (2008). Mechanisms and functional implications of adult neurogenesis. *Cell* **132**, 645-660.

Zhao, B., Tumaneng, K. and Guan, K. L. (2011). The Hippo pathway in organ size control, tissue regeneration and stem cell self-renewal. *Nat. Cell Biol.* **13**, 877-883.

DEVELOPMENT